KSME

Springer

Journal of Mechanical Science and Technology 37 (8) 2023

Original Article
DOI 10.1007/s12206-023-0703-3

Keywords:
· LuGre model
· Friction-induced vibration
· Marine propeller shaft
· Stick-slip behavior
· Dynamical response

Correspondence to:
Qianwen Huang
qwhuang@wust.edu.cn

Citation:
Huang, Q., Xia, J., Liu, H. (2023). Friction-induced vibration of marine propeller shaft based on the LuGre friction model. Journal of Mechanical Science and Technology 37 (8) (2023) 3867~3876.
http://doi.org/10.1007/s12206-023-0703-3

Received November 3rd, 2022
Revised March 17th, 2023
Accepted April 24th, 2023

† Recommended by Editor
No-cheol Park

Friction-induced vibration of marine propeller shaft based on the LuGre friction model

Qianwen Huang[1,2], Jing Xia[1] and Huaiguang Liu[1,2]

[1]Hubei Key Laboratory of Mechanical Transmission and Manufacturing Engineering, School of Machinery and Automation, Wuhan University of Science and Technology, Wuhan 430081, China, [2]Key Laboratory of Metallurgical Equipment and Control Technology, Ministry of Education, School of Machinery and Automation, Wuhan University of Science and Technology, Wuhan 430081, China

Abstract The friction-induced vibration with stick-slip behavior is caused by the contact of the shaft-bearing system. A LuGre friction model is thus applied in the investigation of friction-induced vibration of the marine propeller shaft. The model parameters contain Coulomb friction, stiction force, Stribeck velocity and viscous coefficient are obtained through fitting curves of friction with experimental data in published papers. The dynamical response of a marine propulsion system is measured with an experiment and calculated with the Stribeck model to verify the adaptation of the LuGre friction model in the friction-induced vibration. To capture the nature of the LuGre friction model, the velocity-dependent function, friction coefficient, pre-sliding displacement, hysteresis, break-away force and dynamical response are numerically calculated. The impact factors include relative velocity, tangential force, and rotational speed are discussed with specific comparison. Therefore a suitable model focusing on the friction-induced vibration is proposed for the marine propeller shaft.

1. Introduction

The marine propeller shaft is supported by lubricated bearings and transfers the thrust generated by the propeller to drive the movement of the ship [1]. The fluid pressure provided by the oil film separates the shaft-bearing system to minimize the friction arising from direct contact between these two components [2]. While the lubrication state may change to “boundary lubrication” and even be destroyed with the variation of film thickness due to low rotational speed. The friction-induced vibration (FIV) will be produced between the contact surface [3]. It causes the interaction of the shaft-bearing system to become more complex because of the shaft misalignment caused by heavy loads [4]. The operation condition becomes more serious as enlarged nonlinearity, which may lead to partial fatigue and even overall failures of the transmission system [5]. Therefore, the investigation on friction-induced vibration of the marine propeller shaft has been gradually noticed.

Moreover, the pulsatility of the main engine, the non-uniformity of propeller flow fields and the irregularity of hull deformation [6] will produce external loadings on the shaft. The bearing suffers from unstable lubrication status, edge effect of loadings and even dry friction [7]. The operating conditions of the marine propeller shaft is harsher under low speed, heavy load and start-stop process, which cause the FIV to be more frequent as direct contact of rough surface [8]. It may lead to increased vibration, chattering and noise of the shaft, as well as the rapid wear, heating and even burning of the bearing [9]. The operational reliability of the ship transmission system will be seriously endangered. Thus, it is crucial to find out the basic mechanism to reduce the FIV efficiently.

In order to reveal the coupling mechanism of friction-induced vibration, the investigation of the dynamical response of the stick-slip model [10] is widely applied. The FIV is characterized by discontinuous motion with the slider alternately sticks then slides over the contact surface

[11]. It indicates that the FIV is induced as the dynamic friction is smaller than the static friction, resulting in randomly alternate “stick” and “slip” phenomena [12]. The Runge-Kutta method, modal superposition method [13], modal amplitude stability analysis method [14] and time integration methods were applied for the numerical calculation. Meanwhile, the finite element analysis [15] became famous in this field with the improvement and maturity of computational capability. And related experiments were also conducted to investigate the friction coefficient [16] and stick-slip behavior [17]. It can be concluded that the discontinuity, non-linearity and velocity dependence of the friction coefficients affects the dynamic behavior of the FIV seriously.

Therefore, scholars have carried out extensive research on friction-induced vibrations, including the application of the LuGre model. Wu et al. [18] effectively identify parameters for a LuGre friction model that reflected lateral vibrations caused by velocity based on experimental measures. Muvengei et al. [19] proposed the LuGre friction to model the stick-slip friction at the revolute clearance joints of a multi-body system. Simoni et al. [20] extend the LuGre model for friction-induced vibration to include the effects of dwell time and verify the model with experiments. Zhou et al. [21] presented a modeling method and algorithm for a point contact non-smooth multibody system based on the 2D LuGre friction model. Saha et al. [22] investigated different models of a single-degree-of-freedom system exhibiting friction-induced vibration by modifying the LuGre model. These researches are of great importance in providing a relevant theoretical basis of the LuGre model for the subsequent selection of the FIV [23].

Although the models of quasi-static slip, steady-slip stability, frictionally-damped and energy dissipation have been considered to describe the friction [24]. These investigations involve complex method implementation, high computational costs and strong assumptions of the solution form. Meanwhile, there may be unexpected deviations in solving the process of numerical calculation due to the assumptions of structural stiffness, damping coefficient and other mechanical properties. Considering the intrinsic properties of stick-slip behavior [25] and velocity-dependent characteristics [26], that should be reasonably involved in the theoretical model. Therefore, the most suitable model should be flexible enough to evaluate the FIV with the consideration of the above impact factors.

To address these issues, a LuGre model is proposed to investigate the friction-induced vibration of the marine propeller shaft. The theoretical expression of the model is proposed and a detailed explanation of model parameters is given. The feasibility of the model is validated through a comparison of vibration results between experimental data and the Stribeck model. The features of the model include velocity-dependent function, friction coefficient, pre-sliding displacement, hysteresis, breakaway force and dynamical response of the model are analyzed. The influence of relative velocity, tangential force, and rotational speed are discussed in detail. Finally, a suitable model for the friction-induced vibration of the marine propeller shaft is proposed.

2. Methodology

Fig. 1 shows the schematic of the marine shaft-bearing system and the reaction force between the contact surfaces. Here, the point o is the origin of the coordinate system xoy and the point o' represents the cross-sectional center of the shaft. The F_g and F_n are the gravity and supporting force, the ω is the rotational speed of the shaft. The friction force F_f of the shaft-bearing contact surface can be equivalent to a torque M_f on the shaft.

Considering the torsional vibration of the shaft, the motion equation of friction-induced vibration can be expressed as:

$$j\ddot{\theta} + c_s\dot{\theta} + k_s\theta = M_f \tag{1}$$

where j, c_s and k_s are the moment of inertia, torsional damping and stiffness, respectively. The $\ddot{\theta}$, $\dot{\theta}$ and θ are the torsional acceleration, velocity and displacement.

According to the theoretical formula, the torque M_f is obtained by the multiplication of force and operating distance.

$$M_f = r \cdot F_f \tag{2}$$

where r is the radius of the shaft and F_f is the friction force.

The friction force is proportional to the normal contact force

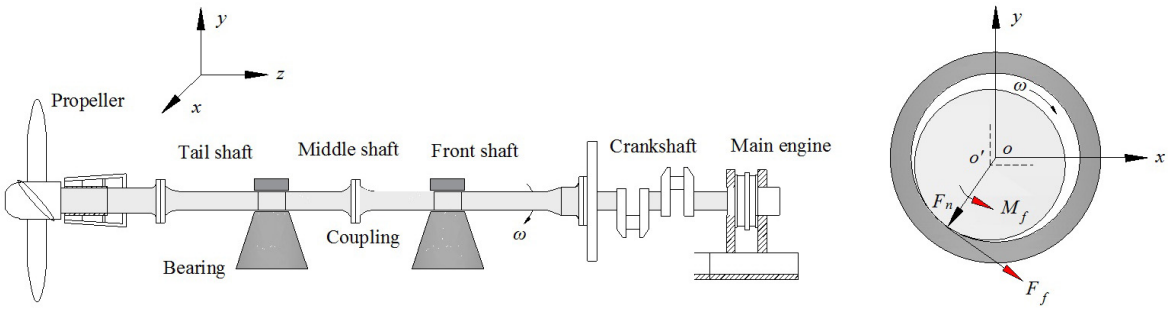

Fig. 1. Schematic of the marine shaft-bearing system and the reaction force between contact surfaces [27].

with a dynamic friction coefficient, which can be expressed as:

$$F_f = \mu(v) \cdot F_n \tag{3}$$

where $\mu(v)$ represents the dynamical friction coefficient with a relative velocity of v. The contact force F_n can be approximately given with statics calculation of shaft gravitation.

The LuGre friction model [28] is based on the average deformation of bristles, which can be applied to represent the lining material of the bearing. The expression of the model is:

$$\begin{aligned} F &= \sigma_0 z + \sigma_1 \dot{z} + \sigma_2 v \\ \dot{z} &= v - \sigma_0 \frac{|v|}{g(v)} z \\ \sigma_0 g(v) &= F_c + (F_s - F_c) e^{-(v/v_s)^2} \end{aligned} \tag{4}$$

where, F is the friction force generated by the motion of the lining material of the bearing, z is the average deformation of bristles with $\dot{z}$ is its derivative with respect to time, v represents the relative velocity of the contact surface, σ_0, σ_1 and σ_2 are the stiffness coefficient, damping coefficient and viscous coefficient of the bristles, respectively. The velocity-dependent function $g(v)$ can reproduce both Coulomb friction and the Stribeck effect with F_c refers to the Coulomb friction, F_s is the level of stiction force and v_s represents the Stribeck velocity.

It can be noticed that the behavior of the LuGre friction model depends on the above-mentioned six parameters: σ_0, σ_1, σ_2, F_c, F_s and v_s. The relationship of friction and velocity with steady-state motion can be expressed as:

$$F_f(v) = F_c \operatorname{sgn}(v) + (F_s - F_c) e^{-(v/v_s)^2} \operatorname{sgn}(v) + \sigma_2 v \,. \tag{5}$$

Here, the dynamical response of the friction will lead to various behavior with a relative velocity that is not constant.

The Dahl's model only accounts for the Coulomb friction F_c can be obtained with an assumption of $\sigma_1 = \sigma_2 = 0$ and $g(v) = F_c / \sigma_0$. The first formular of Eq. (4) can be rewritten as:

$$\frac{dF}{dt} = \sigma_0 v \left(1 - \frac{F}{F_c} \operatorname{sgn}(v) \right). \tag{6}$$

In order to consider the Stribeck effect, the time variable t of the above equation is integrated and then expressed as the displacement variable s. The first-order question can be transformed and replaced by the second-order form:

$$\frac{d^2F}{ds^2} + 2\xi\omega \frac{dF}{ds} + \omega^2 F = \omega^2 F_c \operatorname{sgn}(v) \tag{7}$$

where, ξ is the damping coefficient, the Stribeck effect will be imitated by the change of the motion direction in the velocity $\operatorname{sgn}(v)$.

The average deformation z can be finite to capture the intuitive properties of the LuGre model, and the time derivative of $V(t) = z^2(t)/2$ evaluated along the solution of Eq. (1) can be expressed as:

$$\frac{dV}{dt} = -|v||z| \left(\frac{|z|}{g(v)} - \operatorname{sgn}(v)\operatorname{sgn}(z) \right). \tag{8}$$

It can be expected that the friction will dissipate energy as the dynamical system is dissipative in cyclic motions and thus that the storage function exists. It is dissipative with respect to the function $V(t)$ as:

$$\int_0^t z(t)v(t)dt \geq V(t) - V(0) \,. \tag{9}$$

In order to investigate the insight into the dynamical response of the model in the stiction regime, the moment of inertia of the shaft is defined as j and the torsional angle is given as θ, the equation of motion can be expressed as:

$$j \frac{d^2\theta}{dt^2} = -F = -(\sigma_0 z + \sigma_1 \dot{z} + \sigma_2 v) \,. \tag{10}$$

Linearizing the second formula of Eq. (4) around z = 0 and v = 0, an equation of $d\theta/dt = dz/dt$ can be obtained. The Eq. (10) can be given as:

$$j \frac{d^2\theta}{dt^2} + (\sigma_1 + \sigma_2) \frac{d\theta}{dt} + \sigma_0 \theta = 0 \,. \tag{11}$$

3. Model parameters

It indicates the friction in Eq. (4) is closely related to the values of the impact factors includes F_c, F_s, v_s and σ_2, which can be determined through experiments. A data fitting is conducted on the basis of relative experimental data in Ref. [16]. Four friction materials contain nitrile rubber (NBR), NBR/UHMWPE composites (NU), ultrahigh molecular weight polyethylene (UHMWPE) and polymer resin (PR) are considered with a working temperature of 60 degree centigrade. During the fitting process, the nonlinear least squares method is applied on the basis of the Levenberg-Marquardt algorithm with Bisquare robust. The maximal and minimal change in variables for finite-difference gradients are defined as 0.1 and 1.0e-8, respectively. The function tolerance is defined as 1.0e-6 and the maximal iteration is 400 times.

The results in Fig. 2 shows the friction fitting curves with experimental data and respective residual. It can be noticed that the residual of each case is small enough to ensure the reliability of the fitting. Therefore, the parameter values of the LuGre model includes F_c, F_s, v_s and σ_2 can be obtained, listed in Table 1. Meanwhile, it also proves the LuGre model is suit-

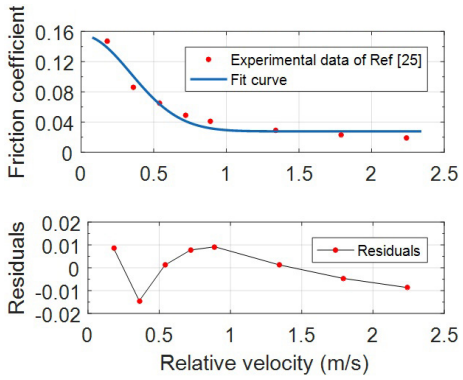

(a) Experimental data and fitting curve

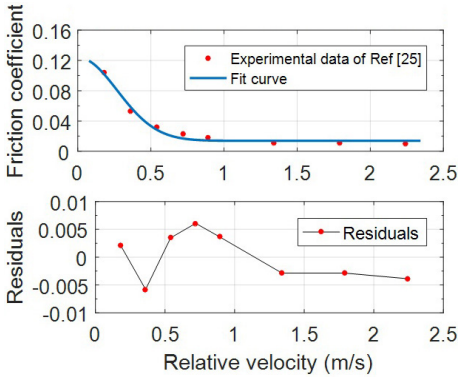

(b) Experimental data and fitting curve

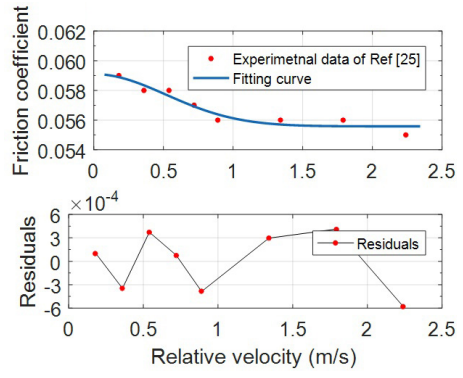

(c) Experimental data and fitting curve

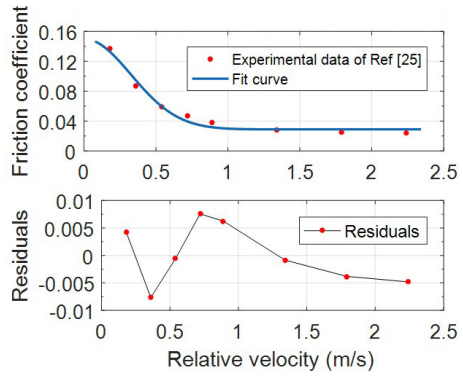

(d) Experimental data and fitting curve

Fig. 2. The friction of the experimental data and the fitting curves: (a) NBR; (b) NU; (c) UHMWPE; (d) PR.

able for estimating friction.

4. Validation

With the LuGre model is testified to be applicable in friction estimation. In order to verify the adaptation in the dynamical response of the marine propeller shaft, vibrations are measured on the experimental platform, shown in Fig. 3. The structure, parameters and more details about the platform can be seen in previous Refs. [29, 30]. The torque of the main engine and the rotational speed of the shaft are defined as 184.8 N·m and 100 rpm. The stiffness coefficient and damping coefficient are defined as $\sigma_0 = 1.0e5\ \mathrm{N}/m$ and $\sigma_1 = 0.02\ \mathrm{N}\cdot s/m$.

The torsional vibration signals of the shaft are achieved by utilizing a laser torsional vibration transducer. A multichannel signal analyzer, which includes servo amplifiers, signal acquisition card and signal output device is arranged to obtain the vibration information. The signal acquisition obtains data from

Table 1. The values of parameters in the LuGre friction model.

Values	Cases			
	NBR	NU	UHMWPE	PR
F_c	0.0610	0.0263	0.0569	0.0496
F_s	0.1799	0.1326	0.0593	0.1609
v_s	0.3316	0.3276	0.5974	0.3775
σ_2	0.0203	0.0083	0.0007	0.0128

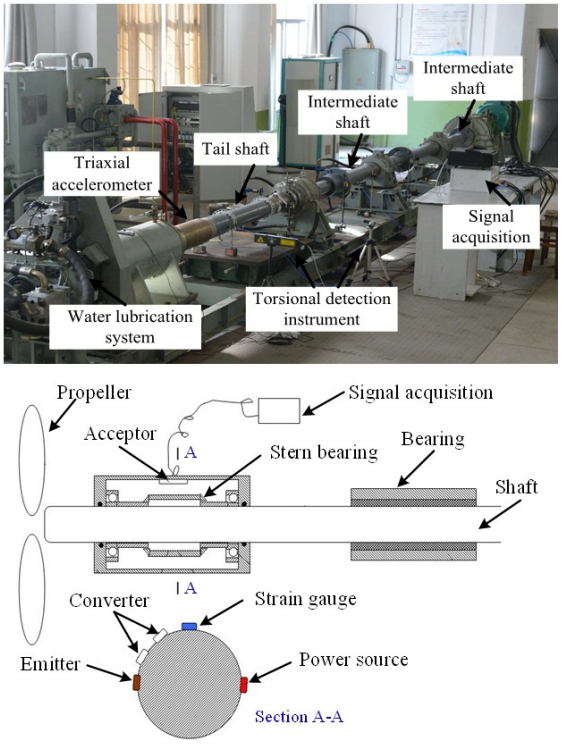

Fig. 3. The diagram of the shaft experimental platform and the schematic of sensor arrangement.

the strain gauge, converter, emitter and acceptor. Moreover, the model parameters of NBR in Table 1 is selected as the lining material of the contact surface.

Fig. 4 shows the comparison of shaft velocity between experimental data and the numerical model. It can be noticed that the results of the proposed LuGre model make a good agreement with experimental data and the Stribeck model. The curves of partial enlargement show nonlinearity at peaks and troughs, which is the stick domain. And the smoother section represents the slip domain during each motion cycle. The stick behavior of the LuGre model is found to be similar with the experiments, especially with that of the Stribeck model.

While a small deviation can still be noticed between these numerical models and experimental data. It may be caused by noise that has not been considered in the numerical calculation. And also, the model parameters assumed in the numerical model. Moreover, the operation status, acquisition method and structural characteristics will lead to a deviation. However, this high confidence level can demonstrate that the LuGre model is applicable in the dynamical estimation.

5. Numerical analysis

With the parameters of the LuGre model is defined through fitting curves of the experimental data, listed in Table 1. And the model is proved to be suitable for the numerical analysis of friction-induced vibration, shown in Fig. 4. On this basis, the investigation focusing on the internal mechanism of the LuGre model is analyzed. The velocity-dependent function, friction coefficient, pre-sliding displacement, hysteresis, break-away force and stick-slip behavior are numerically calculated. Meanwhile, the impact factors of model parameters, relative velocity and rotational speed are discussed in detail.

5.1 Velocity-dependent function

Reminding the friction-induced vibration generally occurred at lower relative velocity The friction coefficient decreases with increasing velocity, as shown in Fig. 2. The influence of model parameters on initial friction coefficient and function $g(v)$ are investigated with the above-mentioned four lining materials. The model parameters in Table 1 are selected and the range of relative velocity from -0.5 to 0.5 m/s is considered.

The results in Fig. 5 are the initial friction coefficient and velocity-dependent function $g(v)$ of the above-mentioned four lining materials of the contact surface. It is interesting to notice that the initial friction coefficient experiences a rapid increase and then slowly decrease with growing velocity. The results make good agreement with the behavior of typical friction force versus speed in previous Ref. [31].

Similarly, the motion of the velocity-dependent function $g(v)$ of the four cases has the same tendency. Specifically, the case of NBR has the largest amplitude of function $g(v)$, the reason may be its largest model parameter of viscous coefficient σ_2. Meanwhile, the case of NBR and NU suffer the fastest drop of function $g(v)$ as the Stribeck velocity v_s contrib-

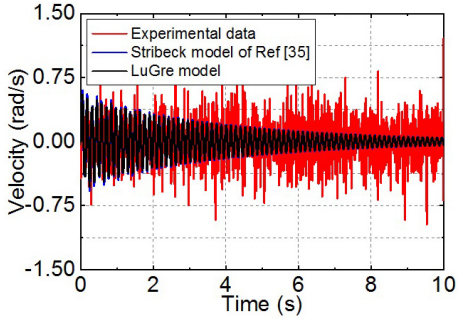

(a) Shaft velocity

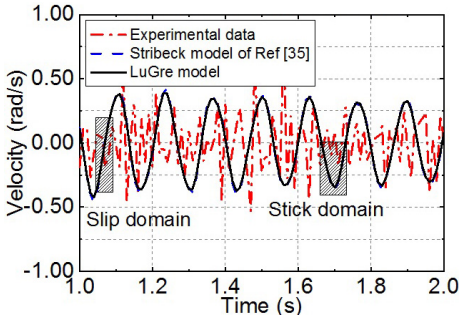

(b) Partial enlargement of (a)

Fig. 4. Comparison of shaft velocity between experimental data and numerical model.

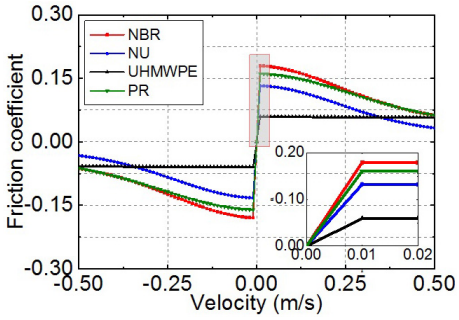

(a) Friction of steady state

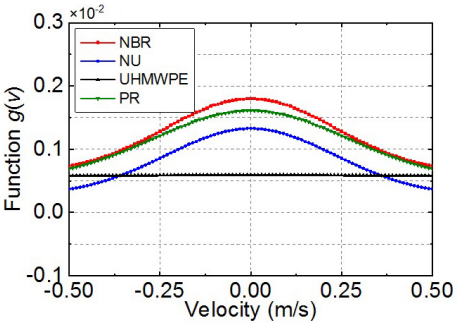

(b) Friction of steady state

Fig. 5. Initial riction coefficient and velocity-dependent function g(v) of friction with steady state.

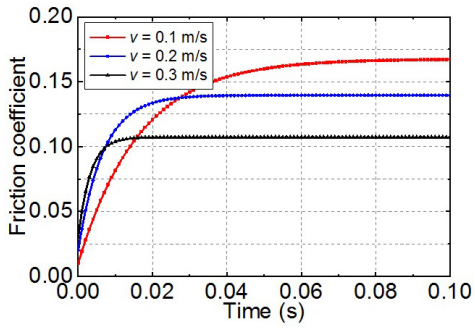

(a) Friction coefficient

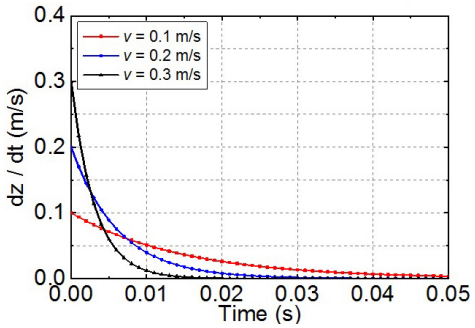

(b) Velocity of deformation z

Fig. 6. The transient behaviour of LuGre friction model: (a) friction coefficient; (b) velocity of deformation z.

utes to the decay rate from maximal value to a stable state. The Coulomb friction F_c and stiction force F_s are found to be relevant to the overall amplitude of velocity-dependent function $g(v)$ as the case of UHMWPE changes the slightest among these cases. Consequently, the FIV with larger σ_2, v_s, F_s and smaller F_c can be considered more potential for friction damage.

5.2 Friction coefficient

The effect of rotational speed on the dynamic friction coefficient is analyzed. For simplification, the velocity is defined as 0.1, 0.2 and 0.3 m/s for possible discussion. The model parameters of the NBR in Table 1 are selected to represent the initial friction coefficient in the numerical calculation. It should be stressed that the rotational speed changes with other parameters remain initial values.

The results in Fig. 6(a) show that the friction coefficient ranges from an initial stationary state to a progressive steady state. As predicted, the friction coefficient is larger with lower velocity, and it also experiences a longer time to reach its steady state. As the relative velocity contains the speed of the lining material of the bearing. The variation dz/dt is analyzed and displayed in Fig. 6(b). It can be noticed that the lining material gradually decays from the corresponding velocity to the steady state, respectively. And the variation of the lowest velocity (0.1 m/s) is noticed to be the slowest, which is the same as the results in Fig. 6(a).

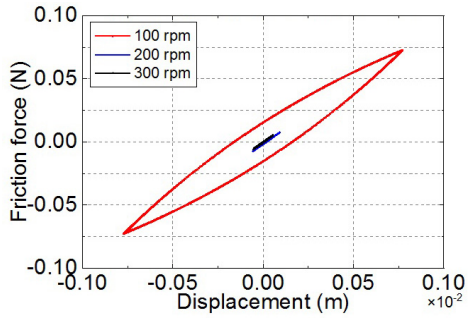

(a) Tangential force with α = 0.1

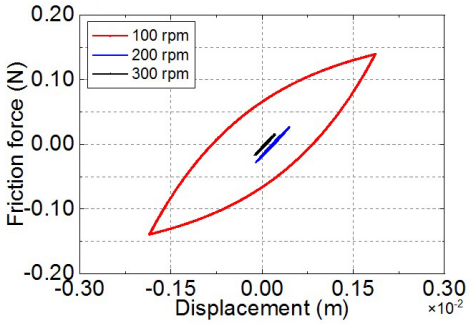

(b) Tangential force with α = 0.5

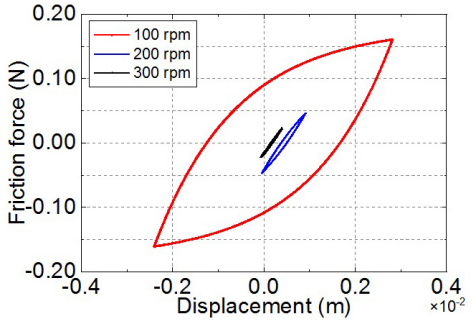

(c) Tangential force with α = 0.9

Fig. 7. Pre-sliding displacement with applied tangential force: (a) α = 0.1; (b) α = 0.5; (c) α = 0.9.

5.3 Pre-sliding displacement

There are usually heavily deformed in the contact region as the shaft and bearing are brought together. The interaction of the surfaces is strong enough that an applied tangential force tending to separate the shaft and bearing will produce displacement in the solid themselves rather than slip in original interfaces. The tangential force is less than the static friction and it will lead to a certain equilibrium displacement. With the increase of the displacement, the tangential force increases slowly and tends asymptotically to static friction [32]. Assuming an external force with various velocities is:

$$F_u = \alpha F_s \cdot \sin(\omega t) . \tag{12}$$

A conversion coefficient α regarding the static friction F_s is defined as 0.1, 0.5 and 0.9. The external force is slowly in-

creased and applied to slide two contact surfaces. The rotational frequency ω is defined as 100, 200 and 300 rpm.

The Fig. 7 shows the pre-sliding displacement of the contact surface with various tangential forces. The friction force is noticed to be a function of closed loops about displacement, which agrees well with published works in Ref. [32]. And the width of the closed curve is more compressed than that of the lower rotational frequency. That means there is a tendency for the contact surface to be separated within a very short displacement. And it is more pronounced to translate into static friction at the contact.

In particular, the pre-sliding displacement is much more sensitive to the rotational frequency. The variation of pre-sliding displacement with the rotational frequency of 100 rpm is found to be much more obvious, over a range of tangential force. Meanwhile, it indicates an enlargement of pre-sliding displacement with increasing tangential force. The maximal pre-sliding displacement in Fig. 7(a) is about 0.075 mm with the tangential force coefficient α = 0.1, while it changes to about 0.3 mm with α = 0.9, shown in Fig. 7(c).

5.4 Hysteresis

The theoretical basis in Eq. (5) indicates that friction varies with velocity. It is found that a multi-valued friction coefficient appeared as a loop about the average (steady state) friction-velocity relation with increasing frequency of oscillation. And a characteristic time delay between changing velocity and friction with the steady state can describe this phenomenon [33]. Therefore, a characteristic time delay is modeled as:

$$v_0 = v \cdot \left(\sin(2\pi\omega t / 60) + 1.5\right). \tag{13}$$

In order to investigate the relationship of friction and velocity, the rotational frequency ω is defined as 100, 200 and 300 rpm with relative velocity v ranges from 0.1 to 0.3 m/s.

The results in Fig. 8 show the hysteresis between the friction force and the velocity. The hysteresis curves can be noticed to be more width with increasing relative velocity, which has been explained through experimental results in Ref. [33]. It can be found that the hysteresis ranges from 0.05 to 0.25 m/s with the velocity is 0.1 m/s, while it changes from about 0.15 to 0.75 m/s with a velocity of 0.3 m/s. For the variety of friction coefficient, the hysteresis ranges from 0.12 to 0.17 with the velocity is 0.1 m/s, while it varies from about 0.04 to 0.16 with a velocity of 0.3 m/s.

Meanwhile, the width of the hysteresis curves is enlarged with increasing rotational frequency. The width with 300 rpm is slightly larger than that of the 100 rpm. It indicates a slight hysteresis of rotational frequency on the friction force.

5.5 Break-away force

The static friction force is the tangential force required to initiate the sliding of the shaft on the contact surface. Assuming there is a force with different rates of increase, the friction force as the shaft starts to slide is the break-away force. Thus, the break-away force can be equated to the friction coefficient of the contact surface.

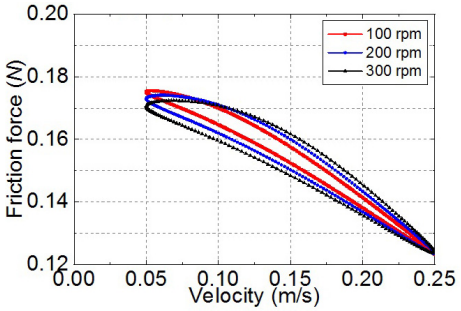

(a) Hysteresis with v = 0.1 m/s

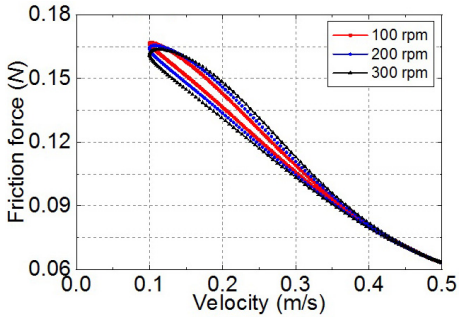

(b) Hysteresis with v = 0.2 m/s

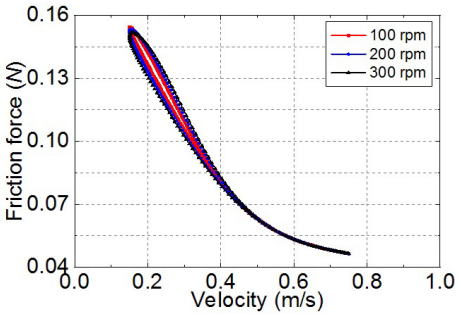

(c) Hysteresis with v = 0.3 m/s

Fig. 8. Hysteresis in friction with various velocity: (a) v = 0.1 m/s; (b) v = 0.2 m/s; (c) v = 0.3 m/s.

The results in Fig. 9 show the break-away force of the system permitted the translation of the peak displacement of the stick-slip cycle into the corresponding maximum tangential force. It can be found that the break-away force decreases gradually with increasing force rate, the stick-slip motion disappears and the pure sliding starts until at approximately 100 N/s of the force rate. The results suggest that the friction coefficient varies between different asymptotes, over a range of rotational speeds. And the higher friction coefficient can be induced with a lower force rate, and vice versa. Meanwhile, the static friction eventually translates into a stable value of friction coefficient with a high force rate. And the time to stabilization is shorter for the case with higher rotational frequency.

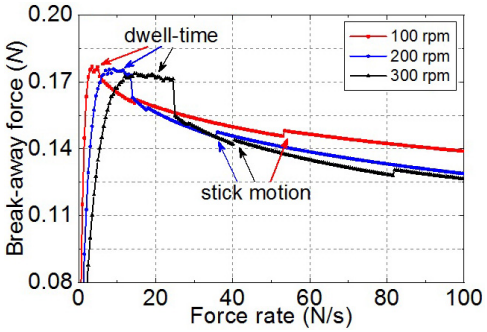

(a) Break-away force with v = 0.1 m/s

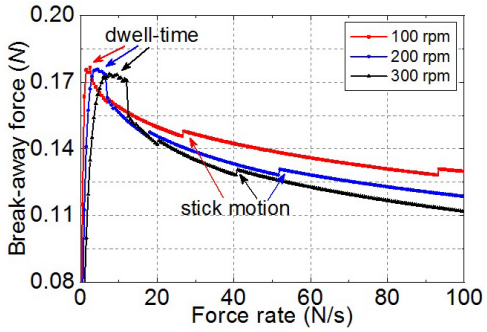

(b) Break-away force with v = 0.2 m/s

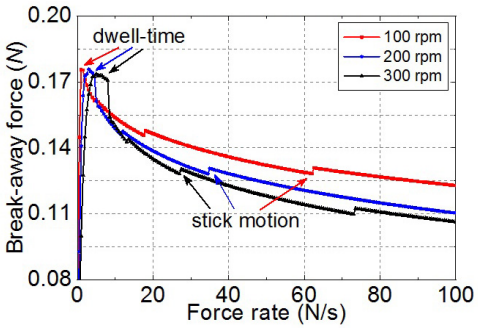

(c) Break-away force with v = 0.3 m/s

Fig. 9. Break-away force with increase rate of applied force: (a) v = 0.1 m/s; (b) v = 0.2 m/s; (c) v = 0.3 m/s.

The dwell-time is the interval during which the contact surface remains static without relative movement in the stick domain. The interval with lower rotational frequency can be noticed to be smaller, especially for the case with 0.1 m/s. The static friction with lower rotational frequency is more likely to transform to slip motion. Moreover, the stick motion can be noticed with discontinuous breaks in the curves of break-away force.

5.6 Dynamical response

The theoretical basis suggests that the stick-slip motion is caused by the friction force at rest being greater than the friction force during rotation. With the applied force reaching the break-away force, which is approximately $\sigma_0 g(0)$, the shaft starts to rotate with pure slip and the friction decreases rapidly as the Stribeck effect. In order to investigate the dynamical response of the friction, the stiffness and damping coefficient is defined as $k = 2N/m$ and ξ = 0.5.

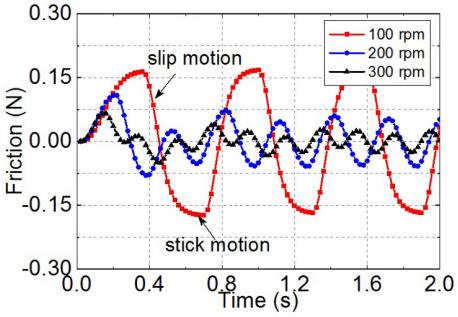

(a) Fricition force

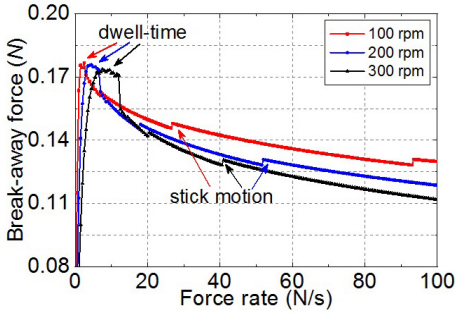

(b) Velocity of dx/dt

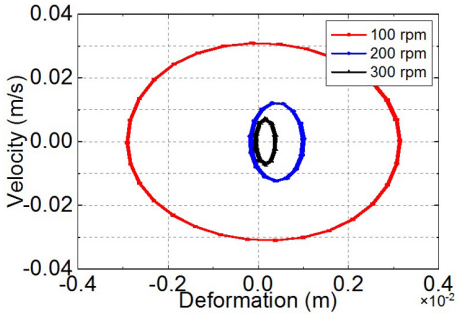

(c) Poincaré diagram

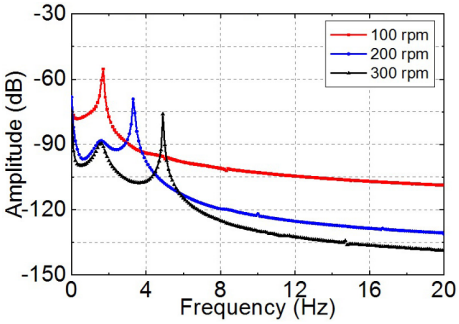

(d) Power spectral density

Fig. 10. Dynamical response of the friction: (a) friction force; (b) velocity; (c) Poincaré diagram; (d) power spectral density.

The Fig. 10 are the dynamical response of force, velocity, Poincaré diagram and power spectral density of the friction. The friction force in Fig. 10(a) can be noticed to be variable as the interaction of the shaft-bearing contact surface. The friction

curve shows slight nonlinearity at peaks and troughs, which is the stick motion of each motion cycle. And the smoother part represents the slip motion. The movement pattern and variation trend of velocity in Fig. 10(b) are found to be much similar to that of the friction. The highly irregular behavior of the friction force can be noticed to be around the region where the velocity is close to zero. The vibration of velocity with 100 rpm is displayed to be much large than that of 300 rpm.

Meanwhile, the dynamical response trends to be stable from the Poincaré diagram in Fig. 10(c). The shape of the Poincaré diagram is not regular circular and trends to be elliptical, which is caused by the interaction of friction and velocity. The frequency of the power spectral density in Fig. 10(d) is about 1.67 Hz, 3.33 Hz and 5.00 Hz, respectively. The results are observed to agree much well for these three kinds of rotational speed.

6. Conclusions

In this research, the LuGre friction model is applied to analyze the friction-induced vibration of the marine propeller shaft. The applicability of the model is validated through the comparison with experimental data and the Stribeck model. The velocity-dependent function, friction coefficient, pre-sliding displacement, hysteresis, break-away force and dynamical response are numerically calculated. The impact factors include relative velocity, tangential force and rotational frequency are discussed in details. Three further contributions can be given:

First, the LuGre model with larger viscous coefficient σ_2, Stribeck velocity v_s, stiction force F_s and smaller Coulomb friction F_c has greater potential for friction damage. A possible range of the parameters is essential to reduce abrasive wear.

Second, the dynamic response of the LuGre model is closely dependent on the relative velocity, especially for the stick-slip motion with lower rotational speed.

Finally, both the pre-sliding displacement and break-away force during friction will be enlarged with increasing tangential force of the contact surface.

In summary, the proposed model is feasible and suitable to be applied in the FIV of the marine propeller shaft. In future work, a more complex model for the FIV will be considered.

Acknowledgments

This work is supported by the National Natural Science Foundation of China (No. 52272377 and 51809201).

References

[1] X. Huang, Z. Su and Z. Zhang, Vibration transmission suppression for propeller-shaft system by hub-embedded damping ring under broadband propeller force, *Nonlinear Dynamics*, 91 (4) (2018) 2651-2666.

[2] Y. Jin, Z. Liu and X. Zhou, Theoretical, numerical, and experimental studies on friction vibration of marine water-lubricated bearing coupled with lateral vibration, *Journal of Marine Science and Technology*, 25 (1) (2020) 298-311.

[3] H. Qin, D. Yang and H. Zheng, Elimination of friction-induced vibration of a propulsion shafting system by auxiliary electromagnetic suspension, *Journal of Vibration and Control*, 26 (17-18) (2020) 1549-1559.

[4] S. Zhu, J. Sun and B. Li, Thermal turbulent lubrication analysis of rough surface journal bearing with journal misalignment, *Tribology International*, 144 (2020) 106109.

[5] W. Qin, H. Qin and H. Zheng, The coupled effect of bearing misalignment and friction on vibration characteristics of a propulsion shafting system, *Proc. IMechE Part M: Journal of Engineering for the Maritime Environment*, 233 (1) (2019) 150-163.

[6] G. Zhang, Y. Zhao and T. Li, Propeller excitation of longitudinal vibration characteristics of marine propulsion shafting system, *Shock and Vibration* (2014) 413592.

[7] X. Shen, J. Jia and M. Zhao, Experimental and numerical analysis of nonlinear dynamics of rotor-bearing-seal system, *Nonlinear Dynamics*, 53 (1-2) (2008) 31-44.

[8] J. Jang and M. Khonsari, On the wear of dynamically-loaded engine bearings with provision for misalignment and surface roughness, *Tribology International*, 141 (2020) 105919.

[9] L. Dong and S. Wang, Research on dynamic characteristic of marine shafting-oil film-stern structure system, *Journal of Dynamic Systems, Measurement and Control*, 141 (2) (2019) 021001.

[10] Z. Zhang, N. Duan and C. Lin, Coupled dynamic analysis of a heavily-loaded propulsion shafting system with continuous bearing-shaft friction, *International Journal of Mechanical Sciences*, 172 (2020) 105431.

[11] M. Stender, M. Bartolomeo and F. Massi, Revealing transitions in friction-excited vibrations by nonlinear time-series analysis, *Nonlinear Dynamics*, 98 (4) (2019) 2613-2630.

[12] H. Han and K. Lee, Experimental verification of the mechanism on stick-slip nonlinear friction induced vibration and its evaluation method in water-lubricated stern tube bearing, *Ocean Engineering*, 182 (2019) 147-161.

[13] C. Wu, F. Chen and X. Long, The self-excited vibration induced by friction of the shaft-hull coupled system with the water-lubricated rubber bearing and its stick-slip phenomenon, *Ocean Engineering*, 198 (2020) 107002.

[14] E. Denimal, J. Sinou and S. Nacivet, Generalized modal amplitude stability analysis for the prediction of the nonlinear dynamic response of mechanical systems subjected to friction-induced vibrations, *Nonlinear Dynamics*, 100 (4) (2020) 3121-3144.

[15] J. Lee, B. Jeong and T. An, Investigation on effective support point of single stern tube bearing for marine propulsion shaft alignment, *Marine Structures*, 64 (2019) 1-17.

[16] J. Huang, X. Zhou and J. Wang, Influence of temperature on friction of polymeric materials in water, *Wear*, 426 (2019) 868-876.

[17] H. Qin, C. Yang and H. Zhu, Experimental analysis on friction-induced vibration of water-lubricated bearings in a submarine propulsion system, *Ocean Engineering*, 203 (2020) 107239.

[18] X. Wu, S. Zuo and L. Lei, Parameter identification for a LuGre model based on steady-state tire conditions, *International Journal of Automotive Technology*, 12 (5) (2011) 671-677.
[19] O. Muvengei, J. Kihiu and B. Ikua, Dynamic analysis of planar multi-body systems with LuGre friction at differently located revolute clearance joints, *Multibody System Dynamics*, 28 (4) (2012) 369-393.
[20] L. Simoni, M. Beschi and A. Visioli, Inclusion of the dwell time effect in the LuGre friction model, *Mechatronics*, 66 (2020) 102345.
[21] Z. Zhou, X. Zheng and Q. Wang, Modeling and simulation of point contact multibody system dynamics based on the 2D LuGre friction model, *Mechanism and Machine Theory*, 158 (2021) 104244.
[22] A. Saha, M. Wiercigroch and K. Jankowski, Investigation of two different friction models from the perspective of friction-induced vibrations, *Tribology International*, 90 (2015) 185-197.
[23] D. Rizos and S. Fassois, Friction identification based upon the LuGre and Maxwell slip models, *IFAC Proceedings Volumes*, 38 (1) (2005) 548-553.
[24] E. Berger, Friction modeling for dynamic system simulation, *Applied Mechanics Reviews*, 55 (6) (2002) 535-577.
[25] C. Dong, L. Shi and L. Li, Stick-slip behaviours of water lubrication polymer materials under low speed conditions, *Tribology International*, 106 (2017) 55-61.
[26] W. Litwin, Influence of main design parameters of ship propeller shaft water-lubricated bearings on their properties, *Polish Maritime Research*, 17 (4) (2010) 39-45.
[27] Q. Huang, H. Liu and Z. Ding, Dynamical response of the shaft-bearing system of marine propeller shaft with velocity-dependent friction, *Ocean Engineering*, 189 (2019) 106399.
[28] C. Canudas, H. Olsson and K. Astrom, A new model for control of systems with friction, *IEEE Transactions on Automatic Control*, 40 (3) (1995) 419-425.
[29] Q. Huang, H. Liu and Z. Ding, Impact factors on friction induced vibration of shaft-bearing system considering stick-slip behavior, *Marine Structures*, 84 (2022) 103226.
[30] Q. Huang, X. Yan and C. Zhang, Coupled transverse and torsional vibrations of the marine propeller shaft with multiple impact factors, *Ocean Engineering*, 178 (2019) 48-58.
[31] A. Krauter, Generation of squeal/chatter in water-lubricated elastomeric bearings, *Journal of Lubrication Technology*, 103 (1981) 406-412.
[32] J. Pratt and E. Eisner, The effect of a tangential force on the contact of metallic bodies, *Wear*, 1 (3) (1957) 529-550.
[33] D. Hess and A. Soom, Friction at a lubricated line contact operating at oscillating sliding velocities, *Journal of Tribology*, 112 (1) (1990) 147-152.

Qianwen Huang is currently an Associate Professor of the School of Machinery and Automation, Wuhan University of Science and Technology. He received his Ph.D. in Marine Engineering from Wuhan University of Technology. His research interests include the mechanics, modeling and measurement of vibrations.